

# Journal of Materials Chemistry B

Accepted Manuscript



This is an *Accepted Manuscript*, which has been through the Royal Society of Chemistry peer review process and has been accepted for publication.

*Accepted Manuscripts* are published online shortly after acceptance, before technical editing, formatting and proof reading. Using this free service, authors can make their results available to the community, in citable form, before we publish the edited article. We will replace this *Accepted Manuscript* with the edited and formatted *Advance Article* as soon as it is available.

You can find more information about *Accepted Manuscripts* in the [Information for Authors](#).

Please note that technical editing may introduce minor changes to the text and/or graphics, which may alter content. The journal's standard [Terms & Conditions](#) and the [Ethical guidelines](#) still apply. In no event shall the Royal Society of Chemistry be held responsible for any errors or omissions in this *Accepted Manuscript* or any consequences arising from the use of any information it contains.

## Monodisperse Photoluminescent and Highly Biocompatible Bioactive Glass Nanoparticles for Controlled Drugs Delivery and Cell Imaging

Yumeng Xue<sup>a</sup>, Yuzhang Du<sup>a</sup>, Jin Yan<sup>a</sup>, Zhengqing Liu<sup>a</sup>, Peter X Ma<sup>a,c,e,f</sup>, Xiaofeng Chen<sup>d</sup>, Bo Lei<sup>a, b, d\*</sup>

<sup>a</sup> Center for Biomedical Engineering and Applied Chemistry, Frontier Institute of Science and Technology, Xi'an Jiaotong University, Xi'an, China

<sup>b</sup> State Key Laboratory for Manufacturing Systems Engineering, Xi'an Jiaotong University, Xi'an, China

<sup>c</sup> Department of Biologic and Materials Sciences, The University of Michigan, Ann Arbor, USA

<sup>d</sup> National Engineering Research Center for Tissue Restoration and Reconstruction, Guangzhou, China

<sup>e</sup> Macromolecular Science and Engineering Center, University of Michigan, Ann Arbor, USA

<sup>f</sup> Department of Materials Science and Engineering, University of Michigan, Ann Arbor, USA

\*Corresponding author:

B Lei, rayboo@xjtu.edu.cn or leiboaray@gmail.com, <http://gr.xjtu.edu.cn/web/rayboo>,

Tel. +86-29-83395361

**Abstract:** Bioactive glass nanoparticles (BGN) have attracted widespread interests recently and been explored as the promising drugs or genes delivery carrier due to their high biocompatibility and tissue repair ability. However, the synthesis of monodispersed photoluminescent BGN and corresponding biomedical applications are still not explored. Here, for the first time, we report monodispersed Eu-doped photoluminescent bioactive glass nanoparticles (BGN-Eu) and demonstrate their biomedical applications for drug delivery and cell imaging. By a long chain amine assisted sol-gel method, we synthesized the monodispersed BGN-Eu with combined dual functions of bioactivity and luminescence property, and further investigated their physicochemical structure, biomineralization activity and biomedical applications. As-prepared BGN-Eu possessed the spherical morphology, relatively homogeneous particle size (200~400

nm) and representative red fluorescent emission characteristic of  $\text{Eu}^{3+}$  at 616 nm. In simulated body fluids (SBF), the BGN-Eu demonstrated excellent bioactivity by inducing biological apatite mineralization. BGN-Eu also presented controlled drug (theophylline) loading ability and release behavior. The osteoblasts (MC3T3) growth was significantly enhanced when incubated with different dosages of BGN-Eu, suggesting the high biocompatibility. In addition, BGN-Eu was successfully used to label MC3T3 cell by a strong red fluorescence with low background noise. Our results suggest the great potential of BGN-Eu as multifunctional bioactive nanomaterials for cell imaging and bone tissue regeneration applications.

**Keywords:** Monodisperse Bioactive Glass Nanoparticles; Photoluminescence; Bioactivity; Biocompatibility; Drug Delivery; Cell Imaging;

## 1. Introduction

Biomedical fluorescent labels and probes have been widely used in cell biological studies and cancer cell diagnostics, provided a nondestructive technique for analyzing cell interactions and molecular mechanism.<sup>1</sup> Conventional fluorescent probes such as organic dyes or proteins, quantum dots, and photoluminescent nanocrystals have been studied and employed in cell and tissue imaging for several years.<sup>2</sup> However, those fluorescent labels have various disadvantages and are limited for large-scale applications. Fluorescent dyes and proteins usually suffer from the high photobleaching and low chemical stability.<sup>3</sup> For inorganic semiconductor quantum dots, there have been wide concerns on their inherent toxicity due to the heavy metal ions components, although they possess excellent photoluminescent properties.<sup>4</sup> Therefore, much effort has been paid to develop new quantum dots such as carbon-based fluorescent nanoparticles.<sup>5</sup> Although carbon-based materials including graphene and carbon dots have stable photoluminescent properties, they still showed potential cell toxicity and tissue toxicity *in vitro* and *in vivo*.<sup>6</sup>

Other photoluminescent materials such as lanthanide-based nanocrystals were also employed for cell

imaging applications in recent years, due to their highly efficient fluorescent properties and low toxicity.<sup>7</sup> In addition, as compared to quantum dots and fluorescent dyes, lanthanide-based nanocrystals possessed high Stokes shift and high chemical/photochemical stability. However, most lanthanide doped nanocrystals including chalcogen chemicals and halogen compounds hold stable crystalline structure and usually exhibited high accumulation in various tissues when used *in vivo*.<sup>8</sup> This high tissue accumulation may produce organ damage and tissue toxicity especially for high dosages and long term use. There is an urgent need to develop a high biocompatible nanomaterial for enhanced bioimaging and disease therapy.

As a non-crystalline material, bioactive glassed (BG) with a typical composition of SiO<sub>2</sub>-CaO have been used in biomedicine including bone tissue repair, tissue substitutes and tissue engineering, due to their high biocompatibility and tissue regeneration ability *in vitro* and *in vivo*.<sup>9-12</sup> BG was also classified to be high bioactive materials based on its high biological apatite-forming ability when soaking in simulated body fluid (SBF).<sup>13</sup> In addition, because of their amorphous structure, BG-based biomaterials have shown controlled biodegradation that Si and Ca ions dissolve and transferred to native apatite in biological environment.<sup>14</sup> The biodegradation and apatite-forming ability make BG high biosafety and biocompatibility in biomedical applications, compared with other nanocrystals including hydroxyapatite, quantum dots and rare earth materials. Therefore, it may be very promising to employ BG nanoparticles (BGN) as novel fluorescent probes or carriers for bioimaging and safe drug delivery.

To carry out broad medical applications in nanomedicine, various BG micro and nanoparticles have been developed by versatile sol-gel process.<sup>15,16</sup> However, due to the amorphous structure and multi-component feature including Si, Ca and P, it is difficult to obtain large-scale and monodispersed BGN by conventional sol-gel methods. Fortunately, recently the large-scale and monodispersed sol-gel BGN were successfully synthesized in our group using dodecylamine as a catalyst and template agent.<sup>17</sup> On the

other hand, biomedical nanoparticles have important applications in drug delivery for enhanced tissue regeneration and disease therapy, as shown everywhere.<sup>18-20</sup> However, functionalized BGN with photoluminescent properties and controlled drug release ability have not been reported yet, although they may have promising applications in bioimaging and drug delivery.

In this study, we firstly report the synthesis of monodispersed and photoluminescent BGN, as well as their applications in drug delivery and cell imaging. The fluorescent ability was carried out by doping Eu (rare earth ion) into BG network. We investigate the physicochemical structure, photoluminescent ability, biomineralization activity, drug loading and controlled release, cytotoxicity and biocompatibility, and cell imaging application of Eu-doped BGN (BGN-Eu).

## 2. Materials and Methods

### 2.1. Materials

Dodecylamine (DDA), Tetraethyl orthosilicate (TEOS), Triethylphosphate (TEP), calcium nitrate tetrahydrate (CN), Europium nitrate hexahydrate (EN) and Ethyl alcohol (99% ETOH) were purchased from Sigma-Aldrich and used without further purification.

### 2.2. Sol-gel Synthesis of Eu doped Bioactive Glass Nanoparticles (BGN-Eu)

The BGN-Eu was synthesized by directly doping Eu into bioactive glass network through dodecylamine (DDA) assisted sol-gel derived method. Here DDA was used as catalyst and template agent to control the monodispersity and nanoscale morphology of BG, which has demonstrated in our previous report.<sup>17</sup> Briefly, 10 g DDA was firstly dissolved in 62.5 ml DW and 200 ml ETOH mixed solution, and stirred until DDA was dissolved completely. 40 ml TEOS was added to the solution with vigorous stirring. After stirring for 30 min, TEP and CN and EN were added to the reaction system in order. The mixture was stirred for 3 h at room temperature. The molar composition of BGN was  $80\text{SiO}_2 : (16-X) \text{CaO} : 4\text{P}_2\text{O}_5 : (X) \text{Eu}_2\text{O}_3$  where X

was denoted as 1, 2, 3 respectively. The obtained white gel was centrifuged, washed by ETOH and water for 3 times, respectively. The product was dried overnight through a freeze-drying method. The dried powders were sintered at 650 °C in air for 3 h. The final samples were named as BGN-Eu0, BGN-Eu1, BGN-Eu2, and BGN-Eu3, respectively.

### **2.3. Physicochemical Structure Analysis of BGN-Eu**

The morphology and size of BGN-Eu was analyzed by transmission electron microscopy (TEM, F20, FEI). The amorphous glass structure was shown by X-ray diffraction (XRD). Fourier transform infrared spectroscopy (FTIR, Nicolet 6700) was employed to determine the chemical structure of nanoparticles. The FTIR spectra were obtained from 4000-400  $\text{cm}^{-1}$ .

### **2.4. Photoluminescent Properties Investigation of BGN-Eu**

The fluorescent property of BGN-Eu was investigated by recording the photoluminescent spectra (PL) (excitation and emission spectra) on a spectrophotometer (F-4500, Hitachi). All samples were tested in water solution with a nanoparticles concentration of 1 mg/mL at room temperature. The fluorescent pictures were obtained by exploring BGN-Eu powder and water solution under UV lamp.

### **2.5. Biomineralization Activity Evaluation of BGN-Eu**

The biomineralization activity was analyzed by soaking samples into simulated body fluids (SBF) for 24 h and 72 h. The SBF with a similar composition with blood plasma was prepared according to our previous report.<sup>21</sup> Typically, the Eu doped nanoparticles were immersed into SBF solution with a concentration of 1.5 mg/mL at 37 °C for different periods. The surface morphology of formed biological apatite nanocrystals on BGN-Eu nanoparticles was observed by TEM. The mineralized apatite crystalline composition and chemical structure was determined by XRD and FTIR respectively.

## 2.6. Drug Loading and Controlled Release Assessment of BGN-Eu

Theophylline (TP) was employed as a model drug to test the drug loading and release behaviors of as-synthesized nanoparticles. Briefly, TP was firstly dissolved in phosphate buffered saline (PBS) to get a concentration of  $5 \text{ mg mL}^{-1}$ . Then 20 mg BGN-Eu was soaked into 2 mL TP solution for 48 hours at  $37 \text{ }^\circ\text{C}$  with a shaking speed of 100 rpm. The TP-loaded BGN-Eu was obtained by centrifuging at 11000 rpm. The resulted samples were washed by PBS to remove the unloaded drug. The loading amount of drug was determined using UV-Vis spectra analysis (Evolution 300, Thermal Sci.). To evaluate the drug release behavior, drug-loaded samples were immersed into PBS with a concentration of  $10 \text{ mg mL}^{-1}$  at  $37 \text{ }^\circ\text{C}$ . At selected time intervals, the solution containing samples was centrifuged, 1 mL supernate was taken out for testing and 1 ml fresh PBS was supplied. The drug concentration was measured by the UV-Vis absorbance at 272 nm through drug standard curves. The drug release behavior was expressed as the cumulative release percentage relative to the releasing time. At least four repeated samples were tested and the result was represented as average value and standard deviation (SD).

## 2.7. *In vitro* Cellular Biocompatibility Analysis of BGN-Eu

The *in vitro* cellular biocompatibility of BGN-Eu were assayed using osteoblast (MC3T3) cell line. Cell line was purchased from Cellbank of Shanghai (Shanghai, China). The cells were cultured in growth medium (DMEM, Invitrogen), supplemented with 10% fetal calf serum (FCS, Invitrogen) in a humidified atmosphere at 5%  $\text{CO}_2$  and  $37 \text{ }^\circ\text{C}$ . The *in vitro* cell cytotoxicity was carried out by culturing cells with BGN-Eu with different concentrations ( $40 \text{ } \mu\text{g mL}^{-1}$ ,  $80 \text{ } \mu\text{g mL}^{-1}$ ,  $150 \text{ } \mu\text{g mL}^{-1}$  and  $250 \text{ } \mu\text{g mL}^{-1}$ ). The nanoparticles solution was prepared by re-dispersing sterilized BGN-Eu into cell growth medium. Briefly, MC3T3 cells were seeded in a 96 well plate at a concentration of 3000 cells per well. After culture for 24 hours, the culture medium was changed to be growth medium containing different concentrations of

BGN-Eu. After another 24 hours, the living cell fluorescent intensity was measured by Alamar Blue kit (Invitrogen) according to the manufacturer instruction. The fluorescent intensity of living cells was assayed through a microplate reader at excitation/emission wavelength of 530/590 nm (SpectraMax, Molecular Devices). The *in vitro* cytotoxicity was expressed as relative fluorescent intensity. The cell proliferation was also evaluated by testing the cell viability using Alamar Blue kit after culture for 2 and 5 days. TCP without BGN-Eu was used as a control. In the cell viability tests, to eliminate the effect of fluorescent nanoparticles, the nanoparticles solution was used as the blank control. At least five species per sample were tested and the data was represented as average value and standard deviation (SD).

### **2.8. *In vitro* Cell Imaging Application of BGN-Eu**

Based on the result of cell cytotoxicity, the BGN-Eu2 solution with a concentration of  $40 \mu\text{g mL}^{-1}$  was used for cell imaging applications. Specially, MC3T3 cells were cultured on coverslips (18mm in diameter) in growth medium for 24 hours. Then cell growth medium was taken out and changed to be fresh medium containing BGN-Eu2. The resulted solution was further incubated for different time periods at  $37^\circ\text{C}$ . At pre-determined time, the coverslips including cells were fetched out, washed by PBS and fixed using paraformaldehyde. The cell fluorescent imaging was investigated by confocal laser scanning microscopy (CLSM, Olympus FV300). The nuclei of the cells were labeled with 4', 6-diamidino-2-phenylindole (DAPI) as an indicator. The staining procedure of DAPI was according to the manufacturer instruction.

### **2.9. Statistical Analysis**

At least four independent tests were carried out and all data were represented as average values and standard deviation (SD). Statistical analysis was performed by a Student's test and the difference was considered as significant when  $*p < 0.05$  and  $**p < 0.01$ .

### 3. Results and Discussion

#### 3.1. Fabrication and Structure of BGN-Eu

Sol-gel process was a very popular method to prepare bioactive glass-based (BG) biomaterials. Bioactive glass nanoparticles (BGN) were also fabricated successfully through template-assisted sol-gel technique developed by our group.<sup>17</sup> In this study, to demonstrate the functionalized biomedical application in bioimaging, Eu doped bioactive glass nanoparticles (BGN-Eu) were developed by modified sol-gel method, as shown in Figure 1. The monodispersed BGN-Eu was formed by adding dodecylamine in the sols containing the precursors of Si, Ca, P, and Eu. Dodecylamine was used as the template molecule and catalyst for assisting the hydrolysis of precursors and gelation of BGN-Eu. The formation mechanism could be found in our previous report.<sup>17</sup> The as-prepared BGN-Eu may have potential biomedical applications in bone tissue regeneration, drug delivery and bioimaging.

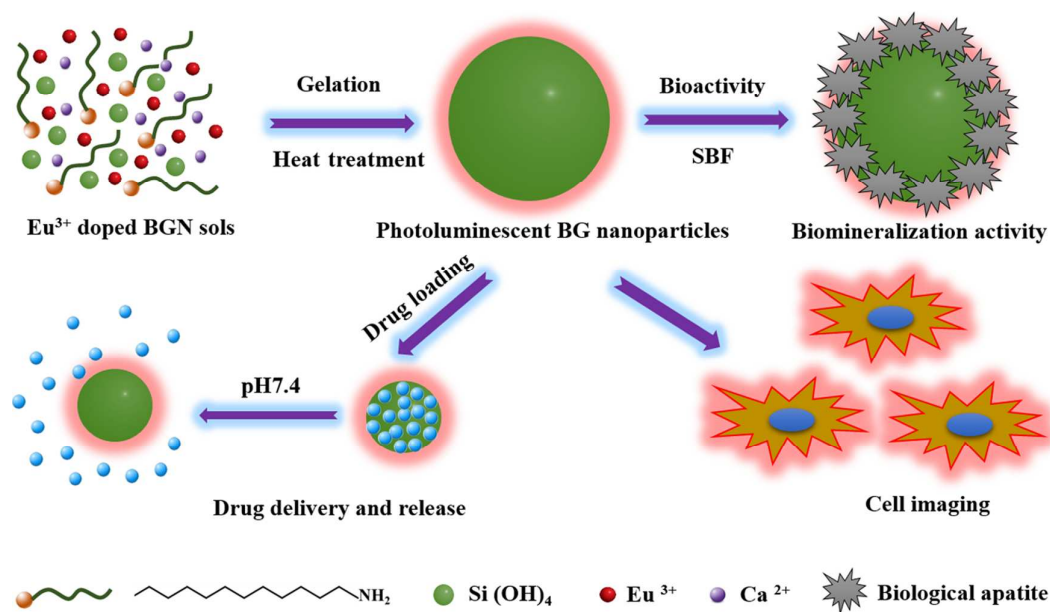


**Figure 1.** Synthetic route and potential biomedical applications of the BGN-Eu.

The as-prepared BGN-Eu possesses a monodispersed spherical morphology and uniform size of 200-300 nm (Figures 2A-D). The functionalized nanoparticles still had the good dispersability in water and

ethanol solution (Supporting Information (SI), Figure S1). The mesoporous structure of BGN and BGN-Eu was also indicated by high magnification TEM images (Figures 2E-H). Sol-gel derived bioactive glass usually possess mesoporous structure after sintering at high temperature, which has been confirmed by pervious reports.<sup>22,23</sup> The Eu incorporation did not produce effect on the morphology and size of functionalized nanoparticles. However, the chemical structure of BGN was significantly changed due to the presence of Eu in BG structure (Figures 2I-J), as shown in FTIR analysis. The broad band at around 1060  $\text{cm}^{-1}$  are associated with the stretch vibration of Si-O-Si, and the peaks at 800  $\text{cm}^{-1}$  and 480  $\text{cm}^{-1}$  were assigned to the bending vibration of Si-O-Si. The bands at 1600-1800  $\text{cm}^{-1}$  and 3300-3600  $\text{cm}^{-1}$  were attributed to the vibration of hydroxyls (-OH). The characteristic bands of Si-O-Si and -OH were significantly weakened as the increase of Eu content, indicating the decrease of bridge-oxygen bonds and glass network integrity. In addition, all samples showed typical amorphous structures although a broad peak at 24° was observed in XRD pattern (Figure 2K). The XRD patterns for different samples were very similar, which demonstrated that the crystalline phase structure of BGN was not affected by Eu (Figure 2K). The X-ray energy dispersive spectroscopy (EDS) test revealed the presence of Eu in BGN structure (SI, Figure S2). These results demonstrated that monodispersed BGN-Eu with uniform size was synthesized successfully by template-assisted sol-gel technique.

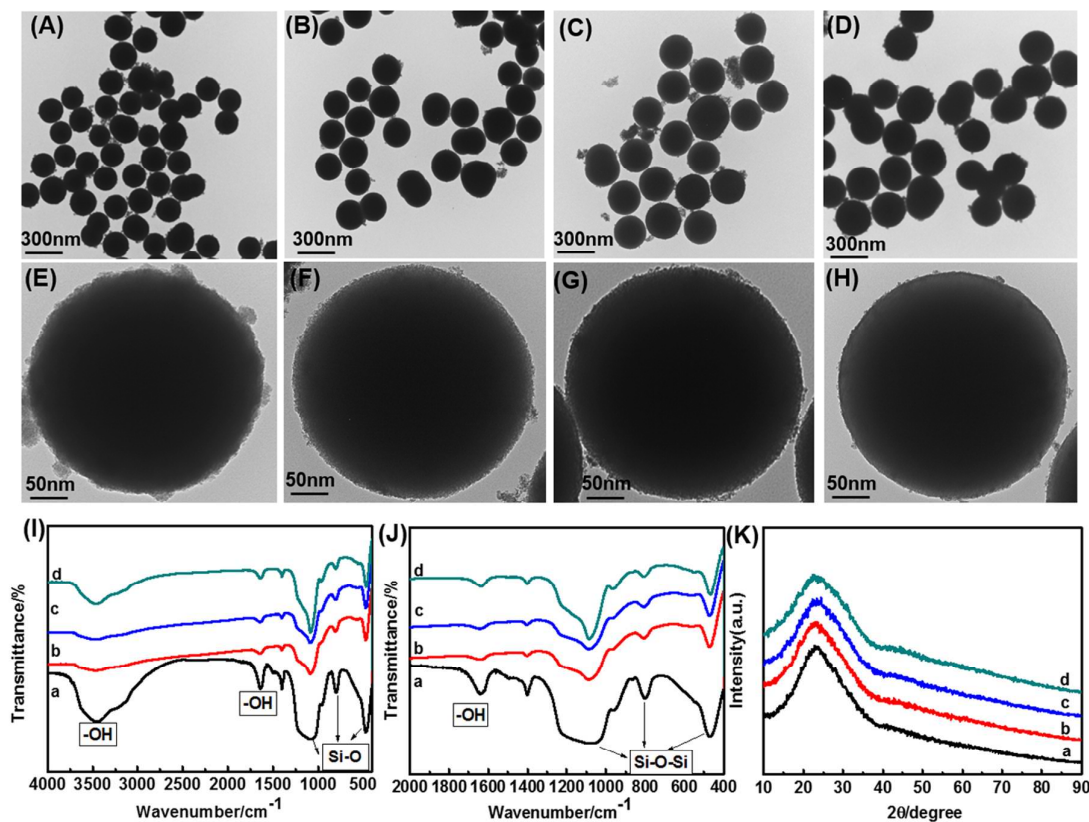


**Figure 2. Morphology and structure evaluation of BGN-Eu.** (A-D) TEM images of BGN-Eu0 (A), BGN-Eu1 (B), BGN-Eu2 (C), BGN-Eu3 (D); (E-H) High magnification TEM pictures; (I, J) FTIR spectra showing the chemical structure of BGN-Eu; (K) XRD patterns indicating the crystalline phase structure of samples (a) BGN-Eu0, (b) BGN-Eu1, (c) BGN-Eu2, (d) BGN-Eu3.

### 3.2. Photoluminescence Properties Evaluation

Due to the excellent photoluminescent properties, the rare earth ions have been employed to prepare photoluminescent nanomaterial. In this study, europium as a rare earth element was doped in structure of BGN to fabricate the functionalized and bioactive nanoparticles for biocompatible bioimaging applications. The photoluminescence properties were investigated by ultraviolet lamp and fluorescence spectrophotometer (Figure 3). Under the irradiation of the UV lamp (254 nm), the BGN-Eu exhibited a representative red emission in both states of powder and dispersed suspension in water (Figures 3A-B). The

red emission brightness significantly increased as the improvement of Eu content. The fluorescent excitation and emission spectra were also investigated, as shown in Figures 3C-D. The BGN-Eu samples showed representative emission wavelengths at 590 nm and 616 nm (5D0—7F2 transition) which were identified as the characteristic of  $\text{Eu}^{3+}$ .<sup>24</sup> The emission peaks intensity significantly increased with the incorporation of Eu, which was in agreement with observation under UV lamp. The photoluminescent ability induced by Eu doping make BGN promising application for bioimaging.

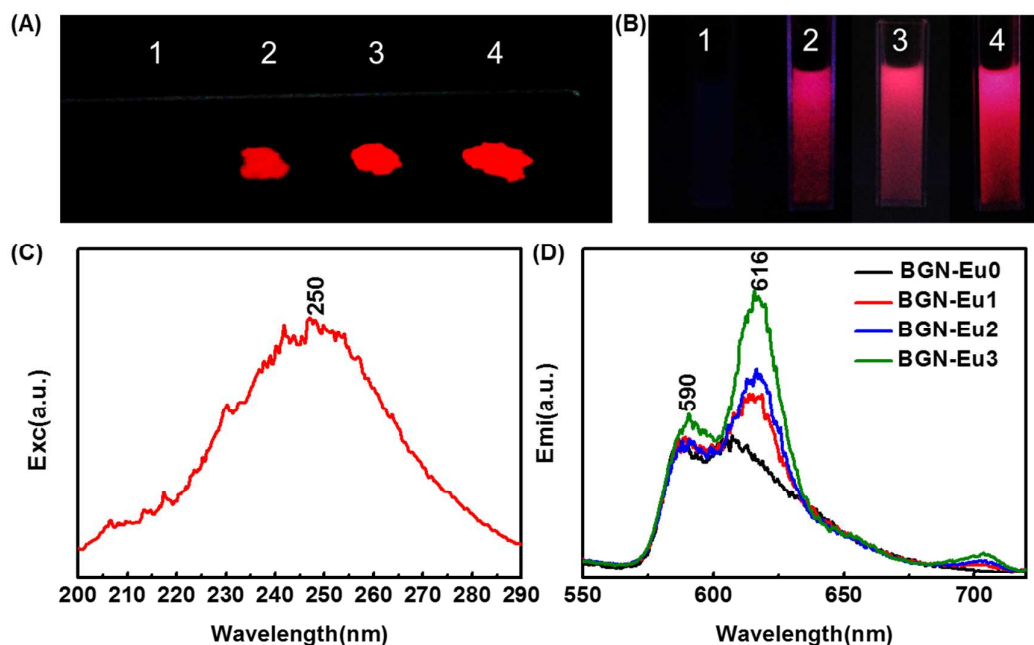


**Figure 3. Photoluminescent properties investigation of BGN-Eu.** (A, B) Fluorescent emission images of BGN-Eu0 (1), BGN-Eu1 (2), BGN-Eu2 (3), BGN-Eu3 (4) under the radiation of the ultraviolet lamp (254 nm); (C) Photoluminescent excitation spectra and (D) Emission spectra of BGN-Eu (excited at 250nm).

### 3.3. Biomineralization Activity Analysis of BGN-Eu

The bioactive glass-based biomaterials usually have good biocompatibility and bone tissue regeneration activity which are probably due to the biological apatite-forming ability (biomineralization activity) under physiological condition. Therefore, the apatite-forming ability was investigated by soaking samples in simulated body fluid (SBF), and analyzed using FTIR, SEM and XRD (Figure 4). After soaking in SBF for

24 hours, new P-O peaks at 562, 605 and 970  $\text{cm}^{-1}$  could be observed from the FTIR spectra (Figure 4A), and these peaks intensity significantly increased as the improvement of soaking time (Figure 4A). XRD measurements further revealed that new peaks attributed to the hydroxyapatite phase were observed at  $26^\circ$  (002) and  $32^\circ$ (211) and  $46^\circ$ (222) after soaking for 24 hours (Figure 4B). Furthermore, these peaks assigned to hydroxyapatite became stronger as increasing soaking time (Figure 4B). TEM images after soaking BGN-E in SBF for 3 days demonstrated that the deposited apatite layer possessed a flake-like morphology (Figures 4C-D). These results clearly showed that our BGN-Eu have excellent biomineralization activity and Eu incorporation did not significantly affect the apatite-forming bioactivity of BGN.

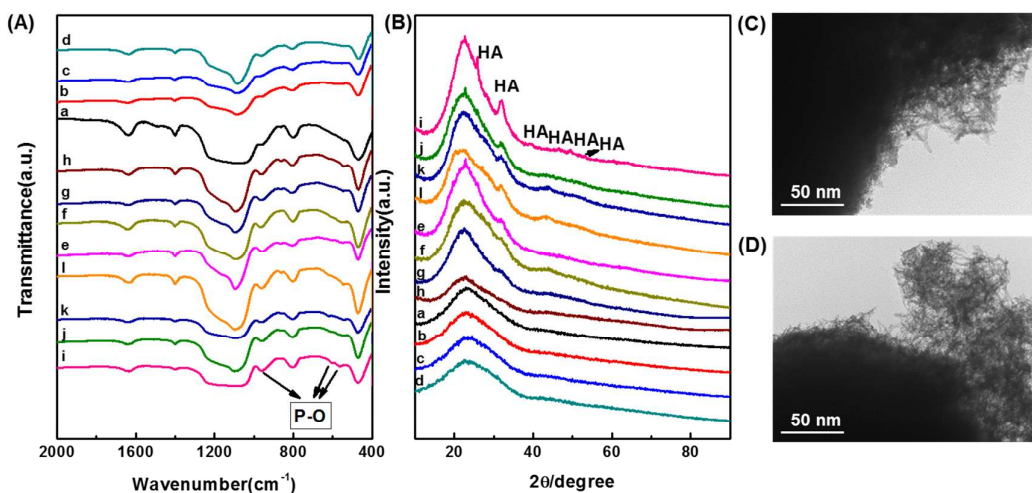


**Figure 4. Biomaterialization activity evaluation of BGN-Eu.** (A-B) FTIR (A) and XRD (B) analysis of BGN-Eu after biomineralization (before mineralization: a) BGN-Eu0, (b) BGN-Eu1, (c) BGN-Eu2, (d) BGN-Eu3; after biomineralization for 24 h: (e) BGN-Eu0, (f) BGN-Eu1, (g) BGN-Eu2, (h) BGN-Eu3; Mineralized for 72 h: (i) BGN-Eu0 (j) BGN-Eu1 (k) BGN-Eu2 (l) BGN-Eu3); (C-D) TEM images showing the morphology of BGN-Eu 2 nanoparticles after biomineralization for 24 h (C) and 72 h (D).

### 3.4. Drug Loading and Release from BGN-Eu

To demonstrate the potential drug delivery application of BGN-Eu, theophylline was used as a model drug to evaluate the drug loading and controlled release behavior of BGN. After loading by BGN-Eu, the

absorbance value of the theophylline solution at 272 nm was significantly decreased, indicating the drug molecules loss adsorption by samples (Figure 5A). The UV-Vis spectra of drug-loaded BGN-Eu solution also revealed the presence of characteristic peak at 272 nm, suggesting the successful drug loading in BGN (Figure 5B). The loading of the drug was further confirmed by FTIR analysis based on the representative characteristic peaks of theophylline (Figure S3). BGN-Eu0, BGN-Eu1, BGN-Eu2, BGN-Eu3 possessed a drug loading content of 3.3%, 3.2%, 3.1%, 2.8% respectively. The drug release behavior was further evaluated by soaking samples in PBS for selected time intervals, as shown in Figures 5C-D. Drugs exhibited controlled release behavior for all samples in 180 min when soaking in PBS at 37°C. It should be noted that there was no significant difference in drug release behavior between different samples in whole immersed periods. Our drug-loading ability and release behavior was comparable with the inorganic nanoparticles-based drug delivery systems.<sup>25</sup> On the other hand, the burst release of drugs were observed, which may be due to the physical loading method and poor interactions between drug and nanoparticles. The initial concentration of the theophylline for nanoparticles adsorption is up to 5 mg mL<sup>-1</sup>, leading to a large proportion of drugs were absorbed on the surface of the particles. When the drug-loaded nanoparticles were soaked in the releasing medium, the drugs absorbed on the surface of the materials were desorbed and then diffused very fast. However, here we just showed the potential application in drug delivery and the delivery efficiency could be improved by loading drugs in the process of biomineralization.

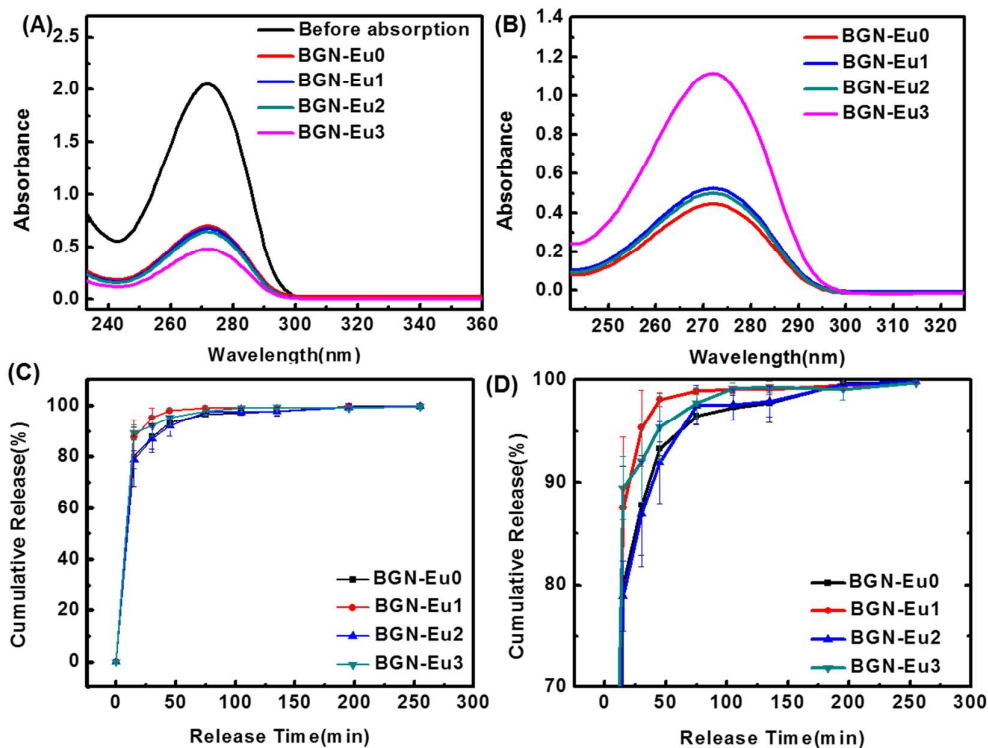


**Figure 5.** Drug loading and release evaluation of BGN-Eu. (A) UV-Vis absorbance spectra of theophylline solution after loaded by nanoparticles; (B) UV-Vis absorbance spectra of drug-loaded nanoparticles in PBS; (C-D) Release behavior of theophylline from nanoparticles after soaking in PBS for 240 min.

### 3.5. *In vitro* Cytotoxicity of BGN-Eu

Although bioactive glass has been accepted as a biocompatible biomaterial in biomedical applications, it is still necessary to evaluate the effect of Eu doping on the cell cytotoxicity of BGN. In consideration of the bone tissue repair and cell imaging applications, osteoblast (MC3T3) was used to analyze the cytotoxicity of BGN-Eu, as shown in Figure 6. After incubation with nanoparticles of various concentrations from 40-250  $\mu\text{g mL}^{-1}$ , the cell viability was higher than TCP control, indicating the low cytotoxicity of BGN-Eu (Figure 6A). For BGN-Eu0 and BGN-Eu3 at high concentration (250  $\mu\text{g mL}^{-1}$ ), the cell viability showed a significant decrease. The cell viability for BGN-Eu2 was significantly increased with increasing particles

concentration, suggesting the high cellular biocompatibility compared to other groups. Suitable trace elements doping concentration including Eu may benefit cell metabolic activity, which was consistent with previous reports.<sup>26,27</sup> In previous report, the cell viability dramatically decreased to be 25% relative to control when the Eu concentration was at 2mM. In our study, the max Eu doping concentration was about 0.3mM in cell culture, therefore, it was reasonable for our nanoparticles to achieve good cell viability.

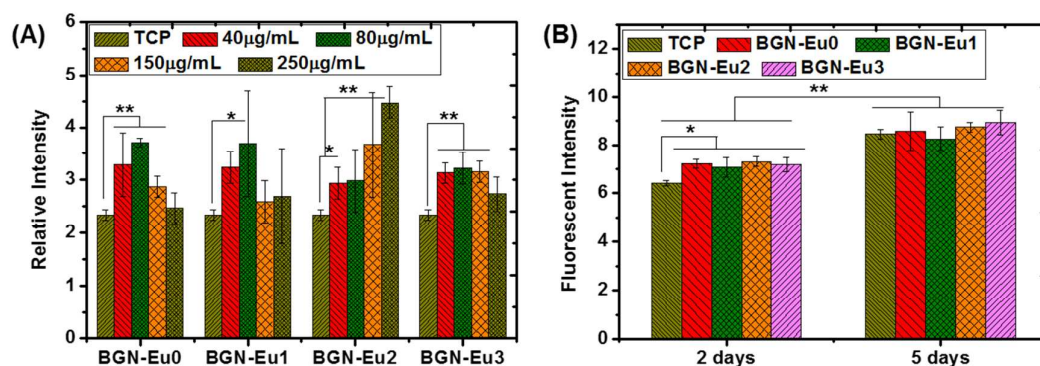


**Figure 6. Cellular proliferation evaluation of BGN-Eu.** (A) Cytotoxicity analysis against MC3T3 cells after incubation for 24h with various concentrations ( $40\text{--}250\ \mu\text{g mL}^{-1}$ ); (B) Cell proliferation in 5 days culture periods after incubation with nanoparticles at  $40\ \mu\text{g mL}^{-1}$ . \* $p < 0.05$  and \*\* $p < 0.01$  was considered as significant differences.

Based on the result of cytotoxicity, BGN-Eu with low ( $40\ \mu\text{g mL}^{-1}$ ) and high ( $250\ \mu\text{g mL}^{-1}$ ) concentration of Eu doping was chosen to evaluate their effect on cell proliferation. As shown in Figure 6B, at  $40\ \mu\text{g mL}^{-1}$ , all samples could support cell growth in the incubation periods of 5 days. Compared with TCP control, at 2 days culture, BGN-Eu significantly enhanced the cell metabolic activity (Figures 6B). After 5 days, only BGN-Eu2 showed the significantly increased cell viability in comparison with TCP, demonstrating that suitable Eu doping could improve cell proliferation. In addition, there was no significant difference between BGN-Eu1 and BGN-Eu3. However, at high particles concentration ( $250\ \mu\text{g mL}^{-1}$ ), no significant difference about the cell viability was observed between different BGN-Eu groups (SI, Figures

S4). The live-dead staining also showed that the cells could efficiently proliferate after culture for 2 and 5 days with nanoparticles at a concentration of  $40\mu\text{g mL}^{-1}$  and  $250\mu\text{g mL}^{-1}$  (Figure 7 and Figure S5). In addition, the cell proliferation behavior of the BGNs after exposure to SBF for 3 days was also investigated, as shown in Figure 8. It is obviously that BGNs post-biomineralization could promote the proliferation of cells, suggesting that the process of the mineralization has little influence on the excellent biocompatibility of the BGNs. Our results demonstrated that BGN-Eu nanoparticles could efficiently enhance osteoblast activity and presented highly cellular biocompatibility which may be a great benefit to their biomedical applications.

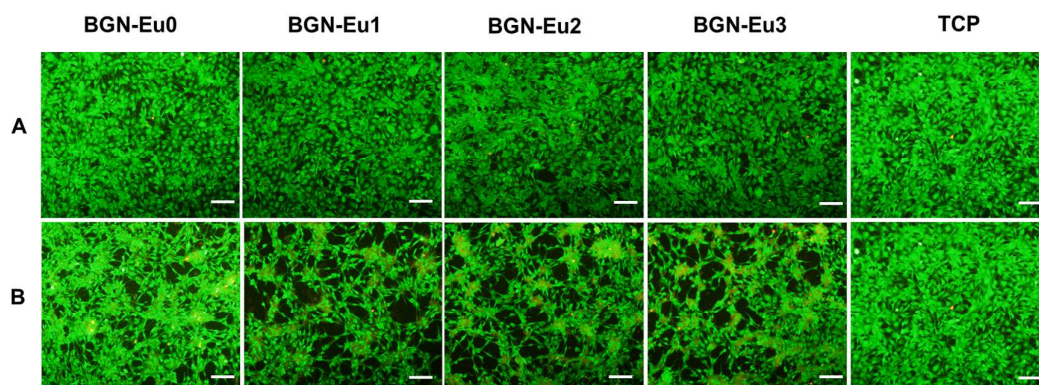


**Figure 7.** Fluorescent images of cells after culture with nanoparticles for 2 days at  $40\mu\text{g mL}^{-1}$  (A) and  $250\mu\text{g mL}^{-1}$  (B) (Scale bar:  $300\mu\text{m}$ ), TCP was used as a control.

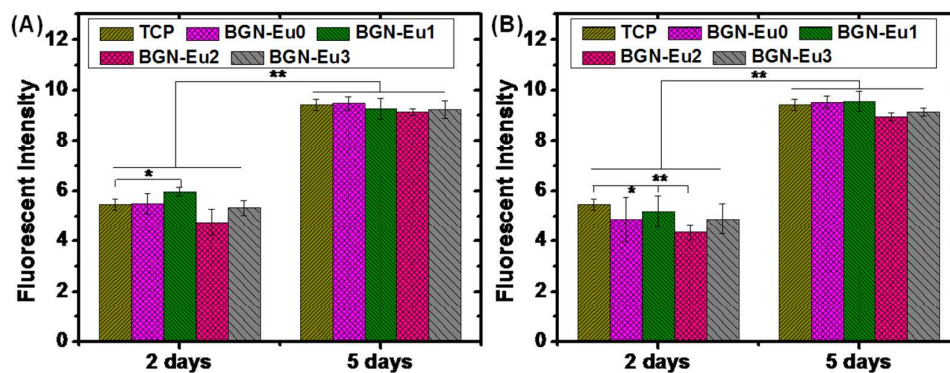


**Figure 8.** Cell proliferation investigation of biomineralized BGN-Eu nanoparticles. Cell viability in 5 days culture periods after incubation with biomineralized nanoparticles at a concentration of  $40\mu\text{g mL}^{-1}$

(A);  $250 \mu\text{g mL}^{-1}$ (B). \* $p < 0.05$  and \*\* $p < 0.01$  was considered as significant differences.

### 3.6. *In vitro* cell imaging of BGN-Eu

To show the application potential in cell imaging, MC3T3 cells were incubated with as-synthesized photoluminescent nanoparticles for different times. Based on the cytotoxicity result and fluorescent properties of BGN-Eu, BGN-Eu2 was chosen to evaluate the cell imaging ability. The fluorescent photographs of MC3T3 cells after incubation with BGN-Eu2 at a concentration of  $40 \mu\text{g mL}^{-1}$  are shown in Figure 9. The cell nucleus was stained as blue by DAPI and the whole cell was stained as red using nanoparticles. During the first 15 min, only a little bit of nanoparticles were taken up by cells and the fluorescence is weak. Most of the red fluorescence existed in cytoplasm. When the incubation time extended to 30 min, it was obviously that more nanoparticles were taken up into the cells and the intensities of the red fluorescence significantly increased. After a further 90 min of incubation, a strong red signal could be observed both in the nuclei and the cytoplasm, indicating that more and more nanoparticles were accumulated in the cells. These results suggested that our BGN-Eu nanoparticles have a good potential for cell imaging applications.

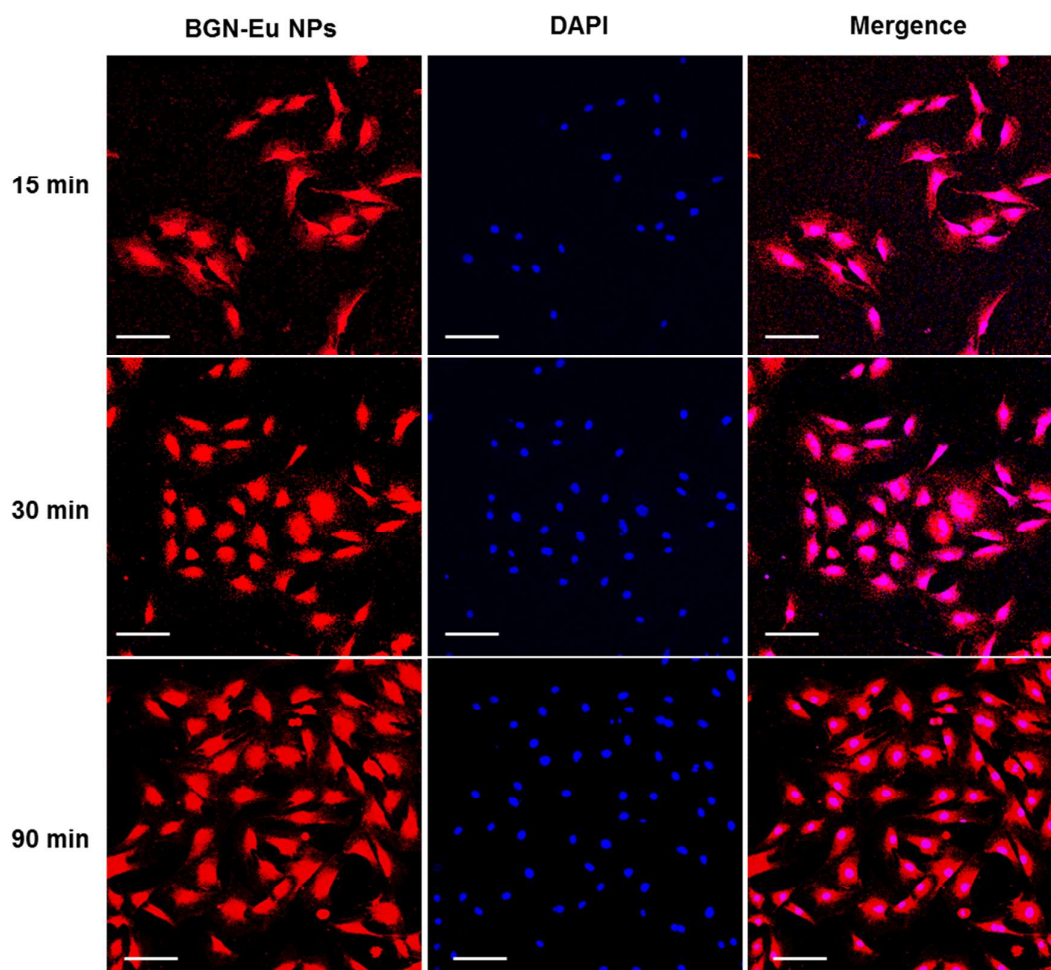


**Figure 9. Cell imaging application evaluation of BGN-Eu.** CLSM images of MC3T3 cells incubated with BGN-Eu1 for 15min, 30min and 90min, respectively. Cell nucleus was stained as blue by DAPI. Cell was stained as red using nanoparticles. The whole cell could be imaged by merging the two channels of red nanoparticles and blue DAPI. Scale bar: 100  $\mu\text{m}$ .

#### 4. Conclusions

In summary, monodispersed and multi-functional europium doped bioactive glass nanoparticles (BGN-Eu) were fabricated by a template-assisted sol-gel method. BGN-Eu showed a uniform spherical morphology with a size of 200-300 nm. After Eu doping, BGN-Eu exhibited a strong red luminescence assigned to the characteristic emission at 616 nm of  $\text{Eu}^{3+}$ . After soaking BGN-Eu into SBF for 24 h, a biological apatite layer could be deposited on surface of nanoparticles, indicating the excellent biomineralization activity.

Drug could be efficiently loaded and underwent the controlled release by BGN-Eu nanoparticles. Our nanoparticles also demonstrated highly cellular biocompatibility by enhancing osteoblast cells proliferation and metabolic activity. The MC3T3 cells could be imaged as red fluorescence through incubation with nanoparticles for different periods. The monodispersed size, good biomineralization ability, photoluminescent property, drug delivery, and high cell biocompatibility make our functionalized nanoparticles promising for bone tissue regeneration and bioimaging applications.

#### Notes:

† Electronic supplementary information (ESI) available.

#### Acknowledgements

We acknowledge the valuable comments of potential reviewers. This work was supported by the scientific research starting foundation from Xi'an Jiaotong University, the Fundamental Research Funds for the Central Universities (XJJ2014090).

#### References

- 1 J. Yao, M. Yang, Y. Duan, *Chem. Rev.*, 2014, **114**, 6130-6178.
- 2 J. Zhang, R. E. Campbell, A. Y. Ting, R. Y. Tsien, *Nat. Rev. Mol. Cell Bio.*, 2002, **3**, 906-918.
- 3 U. Resch-Genger, M. Grabolle, S. Cavaliere-Jaricot, R. Nitschke, T. Nann, *Nat. Methods*, 2008, **5**, 763-775.
- 4 B. A. Kairdolf, A. M. Smith, T. H. Stokes, M. D. Wang, A. N. Young, S. Nie, *Annu. Rev. Anal. Chem.*, 2013, **6**, 143-162.
- 5 K. Hola, Y. Zhang, Y. Wang, E. P. Giannelis, R. Zboril, A. L. Rogach, *Nano Today*, 2014, **9**, 590-603.
- 6 Y. Zhang, S. F. Ali, E. Dervishi, Y. Xu, Z. Li; D. Casciano, A. S. Biris, *ACS Nano*, 2010, **4**, 3181-3186.
- 7 C. Bouzigues, T. Gacoin, A. Alexandrou, *Acs Nano*, 2011, **5**, 8488-8505.

- 8 T. Maldiney, A. Bessière, J. Seguin, E. Teston, S. K. Sharma, B. Viana, A. J. Bos, P. Dorenbos, M. Bessodes, D. Gourier, *Nat. Mater.*, 2014, **13**, 418-426.
- 9 L. L. Hench, J. M. Polak, *Science*, 2002, **295**, 1014-1017.
- 10 B. Lei, X. Chen, Y. Wang, N. Zhao, C. Du, L. Fang, *J. Biomed. Mater. Res., Part A*, 2010, **94**, 1091-1099.
- 11 B. Lei, X. Chen, X. Han, Z. Li, *J. Mater. Chem.*, 2011, **21**, 12725-12734.
- 12 M. N. Rahaman, D. E. Day, B. Sonny Bal, Q. Fu, S. B. Jung, L. F. Bonewald, A. P. Tomsia, *Acta Biomater.*, 2011, **7**, 2355-2373.
- 13 B. Lei, X. Chen, Y. Wang, N. Zhao, C. Du, L. Fang, *Biomed. Mater.*, 2010, **5**, 054103.
- 14 B. Lei, X. Chen, X. Han, J. Zhou, *J. Mater. Chem.*, 2012, **22**, 16906-16913.
- 15 I. Izquierdo-Barba, A. J. Salinas, M. Vallet-Regí, *Int. J. Appl. Glass. Sci.*, 2013, **4**, 149-161.
- 16 B. Lei, K.-H. Shin, D.-Y. Noh, I.-H. Jo, Y.-H. Koh, H.-E. Kim, S. E. Kim, *Mater Sci and Eng: C*, 2013, **33**, 1102-1108.
- 17 Q. Hu, Y. Li, G. Miao, N. Zhao, X. Chen, *RSC Adv.*, 2014, **4**, 22678-22687.
- 18 N. Bertrand, J. Wu, X. Xu, N. Kamaly, and O. C. Farokhzad, *Adv. Drug Deliver. Rev.*, 2014, **66**, 2-25.
- 19 J. Kreuter, *Adv. Drug Deliver. Rev.*, 2014, **71**, 2-14.
- 20 D. Yang, Z. Hou, Z. Cheng, C. Li, and J. Lin, *Chem. Soc. Rev.*, 2015, **44**, 1416-1448.
- 21 B. Lei, X. Chen, Y. Wang, N. Zhao, C. Du, L. Fang, *J. Non-Cryst. Solids*, 2009, **355**, 2678-2681.
- 22 J. R. Jones, L. M. Ehrenfried, L. L. Hench, *Biomaterials*, 2006, **27**, 964-973.
- 23 B. Lei, X. Chen, Y. Wang, N. Zhao, C. Du, L. Fang, *J. Am. Ceram. Soc.*, 2010, **93**, 32-35.
- 24 X. Zeng, J. Yuan, Z. Wang, L. Zhang, *Adv. Mater.*, 2007, **19**, 4510-4514.
- 25 Z.-Z. Li, L.-X. Wen, L. Shao, J.-F. Chen, *J. Control. Release*, 2004, **98**, 245-254.

26 F. Feyerabend, J. Fischer, J. Holtz, F. Witte, R. Willumeit, H. Drücker, C. Vogt, N. Hort, *Acta.*

*Biomater.*, 2010, **6**, 1834-1842.

27 S. Bose, G. Fielding, S. Tarafder, A. Bandyopadhyay, *Trends. Biotechnol.*, 2013, **31**, 594-605.